Broken poloidal symmetry and plasmonic eigenmodes on a torus

Tharindu Warnakula[1,*] Sarath D. Gunapala,[2] Mark I. Stockman,[3] and Malin Premaratne[1,†]

[1]*Advanced Computing and Simulation Laboratory (AχL), Department of Electrical and Computer Systems Engineering, Monash University, Clayton Vic 3800, Australia*

[2]*Jet Propulsion Laboratory, California Institute of Technology, Pasadena, California 91109, USA*

[3]*Department of Physics and Astronomy, Georgia State University, Atlanta, Georgia 30303, USA*

(Received 27 November 2019; revised manuscript received 13 February 2020; accepted 18 February 2020; published 26 March 2020)

We study the poloidal modes (modes whose variations are strictly along the direction of the torus axis) of toroidal nanoparticles. We show that the modes may be understood in terms of the symmetry breaking that occurs when an infinite cylinder is folded to form a torus. This symmetry breaking results in the splitting of the transverse cylinder modes into two distinct sets of modes on a torus. One set of these modes was known to exist already. We show the existence of the second set and also analytically derive the surface charge structure for that set of modes. We also consolidate recent advances made in studying the modal structure on torus particles and complete our understanding of the plasmonic modes of a torus.

DOI: 10.1103/PhysRevB.101.115426

I. INTRODUCTION

The field of plasmonics is concerned with the manipulation of the oscillatory modes of electrons of nanoparticles for confinement, transmission, and amplification of electromagnetic fields [1]. In the last couple of decades, with the advent of advanced experimental and fabrication techniques, the fabrication of nanostructures of ever-decreasing dimensions has become possible, bringing along with it the possibility of controlling electromagnetic fields at the nanoscale. These nanostructures have brought with them exotic possibilities with applications in the fields of chemical sensing through surface-enhanced Raman scattering (SERS) [2], photovoltaics [3], biological sensing [4,5], and imaging [6] applications as well as ultrafast communication systems [7]. In addition to these, applications involving the control of resonance energy transfer between plasmons and emitters at the nanoscale [8], such as spasers [9–13], have been made possible through the advances in nanoscale plasmonics.

The simplest of these nanostructures, the sphere, was analyzed over a century ago and it was shown that the electromagnetic field modes generated take the form of the so called solid harmonics [14]. The surface electron charge modes take the form of spherical harmonics [15] resulting in a structure with threefold-degenerate dipole modes, fivefold-degenerate quadrupolar modes, etc. The structure and behavior of these modes are understood perfectly and a summary of these is presented in Fig. 1; ω_F in the figure is the well known Fröhlich frequency, at which value the permittivity of the material ϵ is such that $\mathrm{Re}\{\epsilon\} = -2$; ω_C is the frequency at which $\mathrm{Re}\{\epsilon\} = -1$. We note here that these exact values only hold when the sphere is placed in vacuum. For general external environments, ω_F is the frequency at which the permittivity of the material has $\mathrm{Re}\{\epsilon\} = -2\epsilon_b$ and for ω_C, $\mathrm{Re}\{\epsilon\} = -\epsilon_b$, where ϵ_b is the permittivity of the environment. One of the key factors understood about the modes on a sphere is that they are normal (i.e., orthogonal): they can be excited independently of each other. Another important factor is that the modes are exactly solvable in the quasistatic limit. Virtually all other plasmonic structures are not solvable exactly and do not possess the property of normality.

Beyond the sphere, in terms of genus, the representative structure in the next level of topological hierarchy is the torus. In plasmonic applications, the torus structure has shown to be incredibly useful as a primary nanostructure allowing for enhanced tuning capabilities compared to spheres [16]. Tori have been shown to possess high-field confinement in the center and also allow for modes with nonzero magnetic dipole moment [17]. As far as analytical characterization of the plasmonic response of a torus goes, it has been known for a while that the Laplace equation is approximately separable in toroidal coordinates [18]. The toroidal (azimuthal) coordinate is completely separable while the other two coordinates are coupled. The first attempts at solving the Laplace equation on a torus surface was carried out in [19,20] in the context of toroidal plasma analysis. In the plasmonic domain, the first attempt at an analysis was done in [17] under certain assumptions. The first complete analysis of the problem was carried out in [21] and [22]. It was also in [21] that the existence of poloidal modes (azimuthally symmetric modes) was first demonstrated. The existence of an infinite class of such modes was shown. In addition to this, plasmonic analyses of modes on a torus were carried out in [16] and [23] within the framework of plasmon hybridization. This formalism described the plasmonic modes on a torus surface as arising from hybridization of primitive plasmons on the inner and outer surface of a torus. However, almost all of these studies focused mainly on toroidal modes, or modes

*tharindu.warnakula@monash.edu

†malin.premaratne@monash.edu

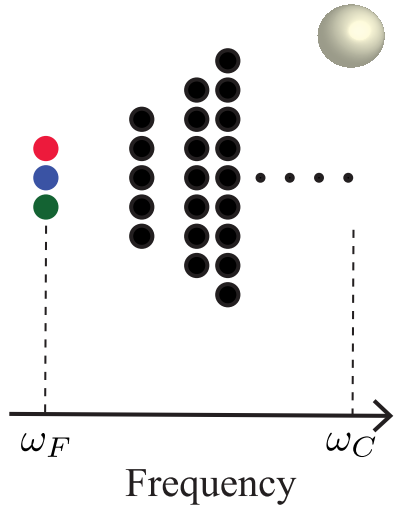

FIG. 1. The plasmonic modes of a sphere. The dipole modes are shown in color and the dark (nonradiative) modes in black. The dipole x mode is shown in red, the y mode in blue, and the z mode in green.

with charge variations in the x-y plane, for a torus with an axis along the z direction. In this paper, we shall focus on the poloidal modes, or modes whose variations are strictly along the direction of the torus axis, and show that the poloidal structure results in numerous amazing hidden properties.

Seemingly unrelated to these developments in fields of physics, it was recently demonstrated that the spectrum of the so-called adjoint Neumann-Poincaré (adjoint-NP) operator on the surface of a torus possesses an infinite number of a negative eigenvalues [24]. The eigenfunctions of the adjoint-NP operator for a given surface are known to furnish the surface charge plasmonic eigenmodes of a particle bounded by that surface, in the quasistatic approximation [15]. The eigenvalues correspond to the resonant permittivities. As we shall show, these eigenmodes with negative eigenvalues actually include an infinite set of poloidal modes which are different from the ones shown to exist in [21]. We shall show that the complete set of poloidal plasmonic modes on a torus may be described as two infinite sets of modes: one set as discovered in [21] with positive adjoint-NP eigenvalues, and another set with negative eigenvalues which we demonstrate here for the first time. We will show that these two sets arise from the breaking of the poloidal symmetry when an infinitely long cylinder is folded to form a torus. By our analysis of these poloidal modes, we complete our understanding of plasmonic modes on a torus.

In the first section of this paper we establish the coordinate systems and derive the poloidal modes corresponding to negative eigenvalues of the adjoint-NP operator analytically. In the next section, we solve the adjoint-NP equation numerically and show the existence of the dual set of poloidal modes and establish the symmetry-broken structure and show that the modes converge to the modes of a cylinder in the low-aspect-ratio limit. In the final section we solve Maxwell's equations and study how the modes overlap and behave under scattering and extinction studies.

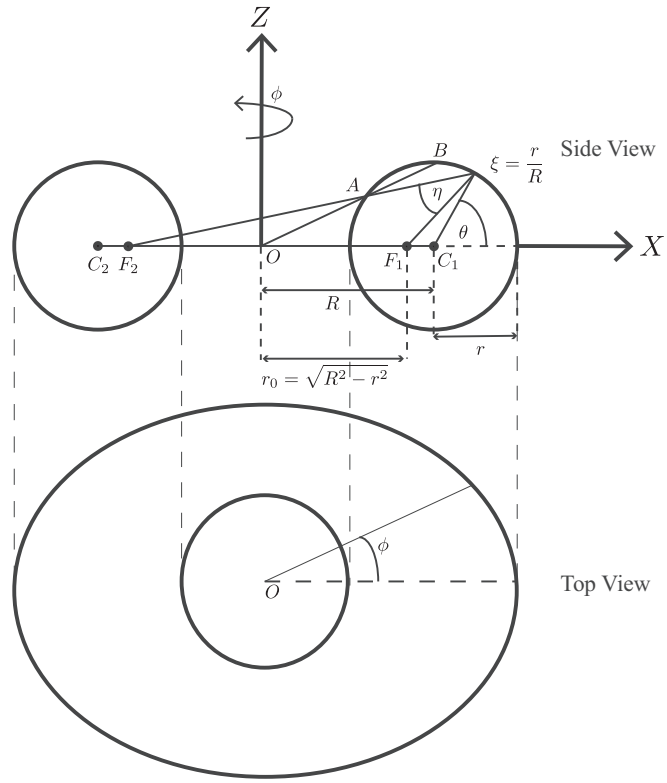

FIG. 2. The toroidal coordinate system and the natural coordinate system on a torus.

II. POLOIDAL MODES ON A TORUS: ANALYTICAL CHARACTERIZATION

We begin our analysis by setting up coordinate systems on a torus. There are two main sets of coordinate systems naturally applicable for tori. The first is the toroidal coordinates (ξ, η, ϕ) as shown in Fig. 2. The figure shows the coordinates as seen from the side of the torus (z-x plane) as well as from the top (x-y plane). Any point on the right half of the z-x plane may be described by the (ξ, η) pair (these two coordinates by themselves are sometimes referred to as the bipolar coordinate system for the plane). Rotating the half plane around the z axis allows us to extend that coordinate system to the whole of 3-dimensional space. The angle ϕ is exactly the azimuthal angle of the spherical polar coordinate system. A torus surface is parametrized by varying (η, ϕ) values and a constant ξ value. We refer the reader to the Appendix for further information on the transformation formulas and other important quantities of the toroidal coordinates.

The second coordinate system is the triplet (ξ, θ, ϕ), which is the natural extension of the polar coordinates to reflect the double-sphere structure ($\mathbb{T} = \mathbb{S}^2$) of the torus. We shall refer to these coordinates as the natural (polar) coordinates. We also note a very interesting property of the toroidal coordinate system here. Performing a geometric inversion [25] of the toroidal coordinates with center at O and radius r_0 furnishes a conformal map from the torus onto itself. Under this transformation, any point A is mapped to the point B as determined by the intersection of the extended line segment OA and the torus surface. This transformation can also be thought of

approximately as a transformation taking the outside surface portion of the torus to the inside and vice versa. This observation will be useful later.

Both the toroidal and natural (polar) coordinate systems are orthogonal. However, it is only in the toroidal coordinates that the Laplace equation is known to have an approximately separable solution. This property was known for a long time and the electric potential field can be expressed as an expansion in terms of the toroidal harmonics [26],

$$\Phi(\xi,\eta,\phi)=\sqrt{1-\xi\cos(\eta)}\sum_{m,n}\begin{Bmatrix}T_{mn}\\S_{mn}\end{Bmatrix}\times\begin{Bmatrix}\cos(m\eta)\\\sin(m\eta)\end{Bmatrix}\times\begin{Bmatrix}\cos(n\phi)\\\sin(n\phi)\end{Bmatrix},\tag{1}$$

where $T_{mn}=\xi^{-1/2}Q^{n}_{m-1/2}(1/\xi)$ and $S_{mn}=\xi^{-1/2}P^{n}_{m-1/2}(1/\xi)$, with Q^{α}_{β} and P^{α}_{β} the associate Legendre functions. The curly braces indicate that any one of the functions within may be chosen to form a valid mode. This equation can be viewed as a modal expansion. The azimuthal direction in a torus is usually referred to as the toroidal direction and the modes that vary in that direction are referred to as toroidal modes. These modes have $m=0$. On the other hand, the direction as labeled by η or θ is the poloidal direction and the modes are referred to as poloidal modes ($n=0$). All other modes are nontrivial superpositions of toroidal and poloidal modes.

As can be seen, the solution is separable in the azimuthal coordinate ϕ due to the corresponding exact symmetry of the torus. This means that the terms in Eq. (1) with different n values are orthogonal. However, the ξ and η coordinates are intrinsically coupled and hence the modes with different m values are not orthogonal. Hence, in general, the toroidal plasmonic response will be a mixture of modes with different m values.

To study the structure of the poloidal modes, we turn to a different formulation of the Laplace equation and the associated boundary value problem: the adjoint Neumann-Poincaré (adjoint-NP) operator. First proposed by Neumann [27] and Poincaré [28] in the context of an extremal value problem, the adjoint-NP operator has recently received much attention in plasmonics as a convenient alternative to the Laplace-equation-based methods [15,29,30]. Consider a bounded object occupying the domain V in $\mathbb{R}^3$ and bounded by surface S with differential surface elements dS and outward-pointing surface normals $n_{\mathbf{x}}$ at coordinates $\mathbf{x}$. Assuming the existence of a source-free charge distribution $\sigma(\mathbf{x})$ on the surface, inducing an electric field inside and outside the object described by $E_0^+(\mathbf{x})$ and $E_0^-(\mathbf{x})$, respectively, we can express the normal components of the electric fields near the surface as [31]

$$n_{\mathbf{x}}\cdot E_0^{\pm}(\mathbf{x})=\mp\frac{\sigma(\mathbf{x})}{2\epsilon_b}+\frac{1}{4\pi\epsilon_0}\int_S\sigma(\mathbf{y})\frac{(\mathbf{x}-\mathbf{y})\cdot n_{\mathbf{x}}}{|\mathbf{x}-\mathbf{y}|^3}dS(\mathbf{y}).\tag{2}$$

The first term on the right-hand side is the contribution of the charge localized at $\mathbf{x}$, to the electric field at $\mathbf{x}$, while the second term is the contribution of the charge dispersed over the rest of the surface. Here, we assume that the permittivity of the surrounding space is given by ϵ_b and that the permittivity of the object is given by ϵ. Now we impose the boundary condition for the continuity of the electric displacement field in the direction normal to the surface, $n_{\mathbf{x}}\cdot(\epsilon E_0^+-\epsilon_b E_0^-)=0$, arriving at

$$\sigma(\mathbf{x})=\frac{\epsilon-\epsilon_b}{\epsilon+\epsilon_b}\frac{1}{2\pi}\int_S\frac{(\mathbf{x}-\mathbf{y})\cdot n_{\mathbf{x}}}{|\mathbf{x}-\mathbf{y}|^3}\sigma(\mathbf{y})dS(\mathbf{y}).\tag{3}$$

This equation expresses the conditions for the existence of the surface charge distribution under source-free conditions. The right-hand side expression is exactly the expression of the adjoint-NP operator $\mathcal{K}^*$ given by

$$\mathcal{K}^*[\sigma](\mathbf{x})=\text{p.v.}\frac{\lambda}{2\pi}\int_S\frac{(\mathbf{x}-\mathbf{y})\cdot n_{\mathbf{x}}}{|\mathbf{x}-\mathbf{y}|^3}\sigma(\mathbf{y})dS(\mathbf{y}).\tag{4}$$

Here p.v. denotes the Cauchy principle value of the integral. The square brackets indicate the fact that $\mathcal{K}^*$ is a functional with argument σ. Setting $\lambda=\frac{\epsilon-\epsilon_b}{\epsilon+\epsilon_b}$, the problem of finding the source-free charge structures on the surface S thus reduces to solving the equation

$$\sigma(\mathbf{x})=\mathcal{K}^*[\sigma](\mathbf{x}).\tag{5}$$

This is an eigenvalue problem of the adjoint-NP operator. It is known that the spectrum of the operator in a smooth domain is real and discrete, and that $\lambda=1$ is one of the eigenvalues. All other eigenvalues have $|\lambda|>1$ [15]. If we let ω_C be the frequency at which $\text{Re}\{\epsilon\}=-1$ of the plasmonic medium, then positive eigenvalues correspond to resonance frequencies $\omega<\omega_C$ and negative eigenvalues correspond to frequencies $\omega>\omega_C$. We use the subscript C here since it is at that very frequency that the transverse plasmonic modes of an infinite cylinder are located (see Fig. 9). For a thorough discussion of the operator equation (5) and its application to plasmonic resonances, we direct the reader to [15] see Eq. (21) therein.

With Eq. (5) in hand, we turn to the torus. We can rewrite the adjoint-NP operator on a torus surface, in toroidal coordinates, as

$$\begin{aligned}&\mathcal{K}^*[\sigma](\eta,\phi)\\&=\int\frac{\kappa\alpha(\eta,\eta')\sigma(\eta',\phi')}{[\mu(\phi-\phi')-\cos(\eta-\eta')]^{1/2}}d\eta'd\phi'\\&\quad-\int\frac{\kappa\alpha(\eta,\eta')\psi(\eta)}{\xi^2}\frac{\sigma(\eta',\phi')[1-\cos(\phi-\phi')]}{[\mu(\phi-\phi')-\cos(\eta-\eta')]^{3/2}}d\eta'd\phi',\end{aligned}\tag{6}$$

where $\psi(\eta)=1-\xi\cos(\eta)$, $\mu(\phi)=1/\xi^2+(1-1/\xi^2)\cos(\phi)$, $\kappa=(1-\xi^2)\psi(\eta)^{1/2}/[8\pi\sqrt{2}\xi\psi(\eta')^{3/2}]$, and $\alpha(\eta,\eta')=\psi(\eta)^{1/2}/\psi(\eta')^{3/2}$. We note that the differential surface element in toroidal coordinates is given by $dS=h_\eta h_\phi d\eta d\phi$, where h_η and h_ϕ are the scale factors in their respective directions. The formulas for the scale factors, normal vectors, and inverse distance in toroidal coordinates are provided in the Appendix.

Observing Eq. (6), we see that the kernel is a function of $(\phi-\phi')$. This is a signature of the exact azimuthal symmetry of the system. This also indicates that Eq. (6) is a convolution operator in the ϕ variable. Functions of the form $e^{ik\phi}$, where k is an integer, are eigenfunctions of such convolution operators [32].

However, the η dependence of the system is much more complicated. While the denominator of the kernel contains terms dependent on $(\eta-\eta')$, there are other terms that

seemingly do not. This structure indicates that the rotational symmetry in the η direction is not exact for the torus. The prefactor terms in Eq. (6) also indicate that the terms of the form $\psi(\eta)^{3/2}$ also seem to be part of the eigenfunctions of the operator. Using these observations we can hypothesize, without loss of generality, that the eigenfunctions should be of the form

$$\sigma(\eta, \phi) = \psi(\eta)^{3/2} e^{ik\phi} g(\eta). \tag{7}$$

With this form, the operator equation reduces to

$$\mathcal{K}^*[\sigma](\eta, \phi) = \kappa \psi(\eta)^{3/2} \int \frac{1}{\psi(\eta)} \frac{g(\eta') e^{-ik\phi'} d\eta' d\phi'}{[\mu(\phi') - \cos(\eta - \eta')]^{1/2}} - \frac{\kappa \psi(\eta)^{3/2}}{\xi^2} \int \frac{g(\eta') e^{-ik\phi'} [1 - \cos(\phi')]}{[\mu(\phi') - \cos(\eta - \eta')]^{1/2}} d\eta' d\phi'. \tag{8}$$

With the inevitable symmetry breaking of the $\psi(\eta)$ functions removed, the kernel still carries a term $1/\psi(\eta)$, which breaks the η symmetry of the resulting eigenfunction (i.e., the kernel still is not a function of exclusively $\eta - \eta'$). To observe the behavior of the kernel for small ξ, we can expand the $1/\psi(\eta)$ term in powers of ξ [this is valid since $|\xi \cos(\eta)| < 1$]:

$$\frac{1}{\psi(\eta)} = 1 + \xi \cos(\eta) + \xi^2 \cos^2(\eta) + O(\xi^3). \tag{9}$$

Taking only the lowest order term, we can rewrite the kernel as

$$\mathcal{K}^*[\sigma](\eta, \phi) = \kappa \psi(\eta)^{3/2} \int \frac{g(\eta') e^{-ik\phi'}}{[\mu(\phi') - \cos(\eta - \eta')]^{1/2}} d\eta' d\phi' - \frac{\kappa \psi(\eta)^{3/2}}{\xi^2} \int \frac{g(\eta') e^{-ik\phi'} [1 - \cos(\phi')]}{[\mu(\phi') - \cos(\eta - \eta')]^{1/2}} d\eta' d\phi'. \tag{10}$$

This kernel is a function of $\eta - \eta'$ and has exact η symmetry. Hence we can describe the eigenfunction $g(\eta) = e^{il\eta}$. This gives us the form of the approximate eigenfunctions as

$$\sigma(\eta, \phi) = \psi(\eta)^{3/2} e^{ik\phi} e^{il\eta}. \tag{11}$$

This implies that, apart from the $\psi(\eta)$ term, the eigenfunctions have sinusoidal dependence on both angular variables η and ϕ. Since we are exclusively interested in poloidal modes, we set $k = 0$ and derive the following modes:

$$\sigma_l^S(\eta) = \psi(\eta)^{3/2} \sin(l\eta), \tag{12a}$$

$$\sigma_l^C(\eta) = \psi(\eta)^{3/2} \cos(l\eta). \tag{12b}$$

σ_l^S is antisymmetric and hence will have a net dipole moment while σ_l^C will be dark. We refer to those modes that do not radiate into the far field as dark modes. We plot both charge distributions in Fig. 3. As can be seen, the charges are mainly localized to the internal "gap" of the torus. We term these modes internal modes, or I modes, due to this behavior. We also label the individual modes as either IS_l or IC_l modes, depending on the sine or cosine structure. We further observe from Eqs. (12) that for smaller ξ, the two modes reduce to the usual sine and cosine cylinder modes. As shown in Fig. 3, for larger ξ values, the charge distributions of the modes seem to accumulate near the $\eta = \pi$ point.

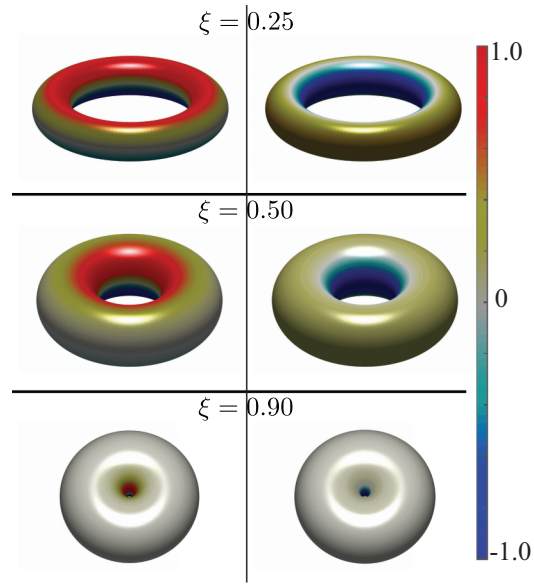

FIG. 3. The charge distributions of the IC_1 and IS_1 modes as described by Eqs. (12) at various aspect ratios.

III. POLOIDAL MODES ON A TORUS: NUMERICAL CHARACTERIZATION

Now we turn to the numerical solution of the adjoint-NP operator equation. For this purpose, we can reinterpret Eq. (4) as an equation involving solid angles between discretized surface elements $\{\mathbf{x}_i\}$ [15],

$$X_i = \frac{\lambda}{2\pi} \sum_j \omega_{ij} X_j. \tag{13}$$

Here, X_i is the total charge on the ith surface element and ω_{ij} is the solid angle subtended on the jth surface element, by the ith element. The problem can thus be cast in the form of an eigenvalue equation and solved efficiently. For further information on the numerical technique and the algorithm, we direct the reader to [15] (see Sec. VI therein). We note that the equation is not referred to as the adjoint-NP operator in [15], but instead generally referred to as Eq. (21). We solve this equation and confirm the existence of the I modes we analytically derived earlier. We show the lowest order modes for $\xi = 0.5$ in Fig. 4. The eigenvalues of these modes turn out to be all negative and hence the resonance frequencies $\omega > \omega_C$. The negativity of the eigenvalues may be linked to the negative Gaussian curvature of the inside surface of the torus, where the charge distribution of these I modes is concentrated. Given a surface element δ_i on the inside surface of a torus, the ω_{ij} angles subtended by most other surface elements δ_j on the inside surface are negative. Hence the sum of Eq. (13) is negative, resulting in a negative eigenvalue. We also note here that in [33], it was proven that given a smooth surface with a region with negative Gaussian curvature, the adjoint-NP spectrum of that surface, or of the surface formed by an inversion, has negative eigenvalues. Given the natural inversion from the torus onto itself that we described earlier, this suggests that the adjoint-NP spectrum of the torus will contain negative eigenvalues. This observation also reinforces

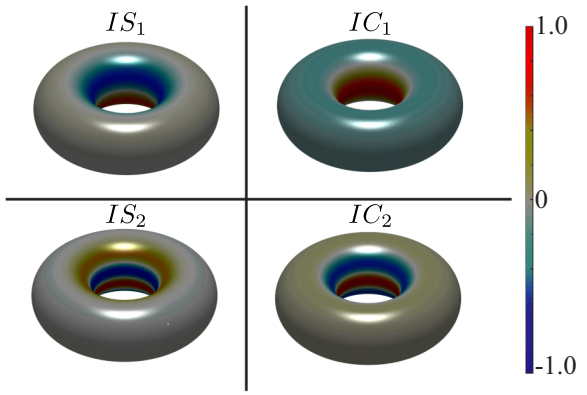

FIG. 4. The charge distributions for the lowest order I modes at $\xi = 0.5$.

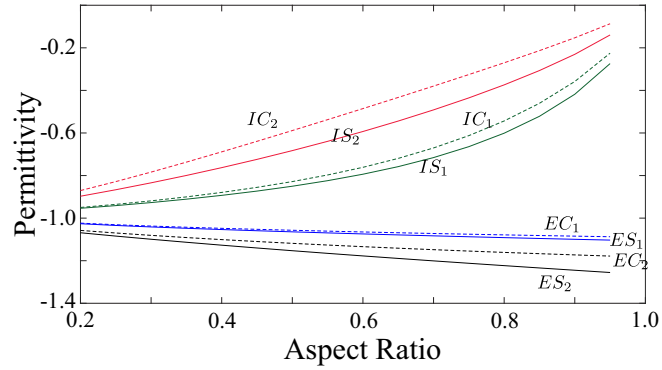

FIG. 6. The resonance permittivity values of the lowest order I and E modes at various aspect ratios.

the importance of the negative curvature portion of the surface to the existence of the negative eigenvalue mode and the corresponding I mode.

In addition to these modes, we discover another set of modes with charge distributions concentrated on the outside surface of the torus. These modes have positive eigenvalues. The positive eigenvalues can be linked to the positive curvature of the outside surface of the torus where the charges are concentrated. We label these modes exterior modes, or E modes. Similarly to the I modes we also label them based on the symmetry or asymmetry structure with labels ES_l and EC_l. Figure 5 displays the lowest order of these modes for $\xi = 0.5$. Unlike the I modes, the E modes do not display a strong variation of the extent of the charge distribution with changing ξ. There is however a very minor effect of accumulating toward the $\eta = 0$ point with increasing ξ.

Next we study the resonance permittivities of the two sets of poloidal modes (Fig. 6). As can be seen, the I modes have permittivities $\epsilon > -1$ while the E modes have $\epsilon < -1$. In [21], the solution of the Laplace equation only established the existence of the lower branches corresponding to the E modes. We also note that the permittivities tend to -1 as the aspect ratio ξ is reduced. This is due to the fact that in the infinitely thin torus limit, the torus structure tends, at least locally, to that of an infinite cylinder. In that limit, the poloidal modes tend to the transverse plasmonic modes of a cylinder. We note that all of the transverse modes of a cylinder are located at frequency ω_C. Hence, this graph hints that the two sets of modes may be considered as originating from the splitting of the transverse modes of a cylinder.

We confirm this hypothesis in Fig. 7, where we plot the charge distribution of the ES_1 and IS_1 modes at different ξ. We see that both of the charge distributions tend toward the charge distribution of a transverse z-dipole mode of a cylinder for smaller ξ. This reestablishes that the two sets of modes are actually manifestations of the symmetry breaking that occurs when a cylinder is folded to form a torus. Similarly, the EC_1 and IC_1 modes approach the charge distribution of the x-dipole mode of a cylinder (for a dipole with axis along the y axis).

Next we study the dipole moments of the asymmetric modes we have discovered. The dipole moments of dipole-active modes dictate the majority of the interactions the particle will have with incident light. We plot the first two I and E modes in Fig. 8. We note that the relative values of the dipole

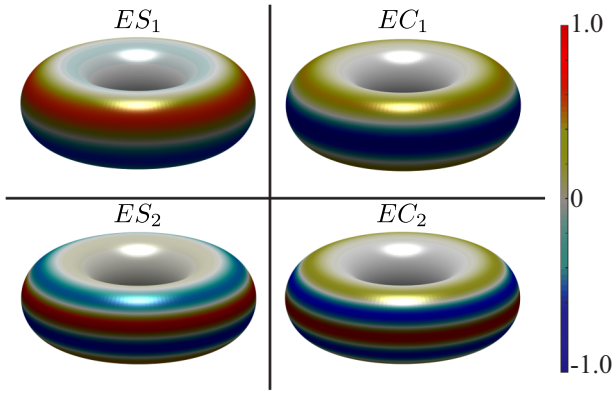

FIG. 5. The charge distributions for the lowest order E modes at $\xi = 0.5$.

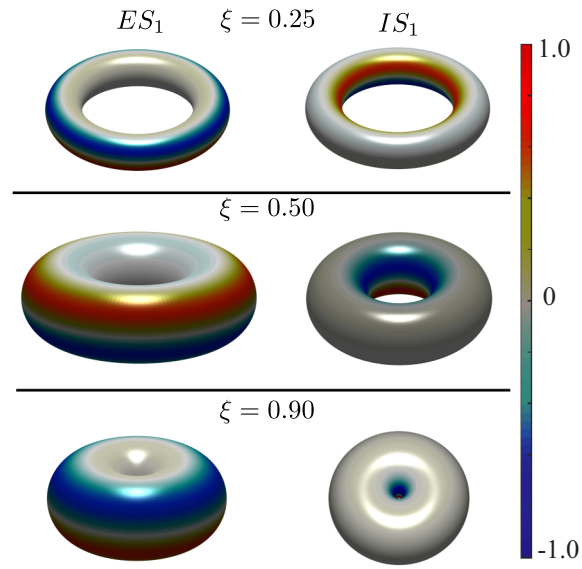

FIG. 7. The charge distributions of the ES_1 and IS_1 modes at various aspect ratios.

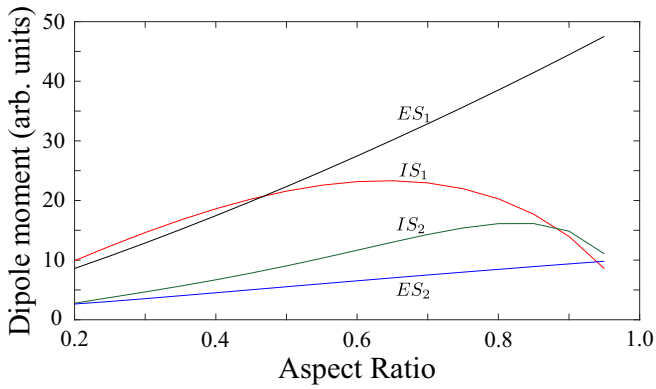

FIG. 8. The dipole moments of the lowest order dipole active I and E modes at various aspect ratios.

moments have not been normalized and hence comparisons should not be drawn between the curves but instead within the curve itself. E modes show a linear variation in the dipole moment. This can be understood by considering that the charge distribution shape of the E modes shows relatively small variation while the minor radius of the torus increases. This results in a linear increase of the dipole moment with ξ. On the other hand, the I modes display a linear progression at low ξ values. But for higher ξ, the charge distribution accumulation at $\eta = \pi$ causes a reduction in the spread of the charges in the z direction leading to smaller dipole moment values.

In Fig. 9 we illustrate this splitting clearly showing the transverse modes of the cylinder as extracted from the adjoint-NP operator formalism, along with the modes of the torus. The z-dipole mode of the cylinder splits into the ES_1 and IS_1 modes while the x-dipole mode splits into the EC_1 and IC_1 modes.

With the complete characterization of the poloidal modes that we have established up to now, we are ready to present the full spectrum of the torus eigenmodes. In Fig. 10, we present the full spectrum of the torus which is the counterpart of the spectrum of the sphere given in Fig. 1. The z-dipole modes are denoted in green, with the x modes in red and y modes

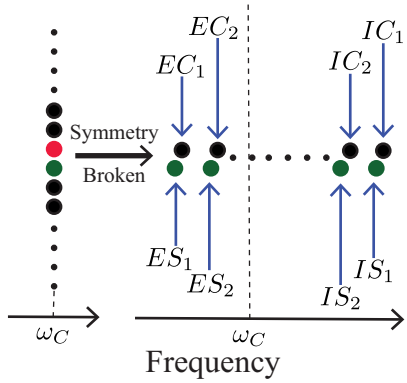

FIG. 9. The splitting of the transverse cylinder modes into the dual set of torus modes. Specifically, the z-dipole mode splits into the ES_1 and IS_1 modes while the x-dipole modes splits into EC_1 and IC_1.

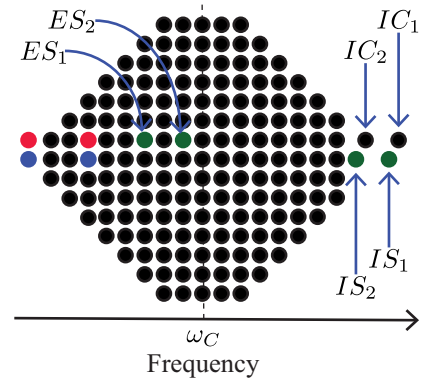

FIG. 10. The complete spectrum of a torus. The dipole modes are shown in color while the dark modes are black. The dipole x mode is shown in red, the y mode in blue and the z mode in green.

in blue. The I modes are the highest frequency modes in this figure. For smaller ξ values, the I modes will recede into the dark-mode continuum and for larger ξ values, more I modes emerge from within the dark modes. The E modes remain hidden deep within the dark modes. Their detuning from ω_C is also smaller as compared to the corresponding I modes. The toroidal modes with dipole moment in x and y directions are the lowest frequency modes on the torus. Unlike the I modes, they remain the lowest frequency modes irrespective of the value of ξ. Higher order dipole-active toroidal modes arise from the superposition of the toroidal modes with symmetric poloidal modes. The first of these dipole-active modes are also shown in the figure. All of these modes tend toward ω_C for smaller ξ.

IV. POLOIDAL MODES ON A TORUS: MAXWELL'S EQUATIONS

While we have performed an analysis of the complete modal structure of the poloidal modes, one important factor that affects the relevance of these modes to understanding the behavior of toroidal particles under electric fields is the fact that the modes are not orthogonal. For a spherical particle, the derived modes are completely orthogonal and hence they can be analyzed individually. However, on a torus, the poloidal modes are all coupled to each other such that all ES_l and IS_l modes are coupled to each other. Similarly the IC_l and EC_l are coupled as well. Hence, in general, it is a linear combination of these modes that will be excited depending on the excitation source. However, if the modes are detuned far enough in frequency space, and the excitation source is at a specific frequency, only the modes local to the excitation frequency will be excited. As we saw earlier, the lower order IS modes are quite detuned from the rest of the torus spectrum for high enough values of ξ. Hence they may be excited individually under such conditions.

To study this behavior, we solve Maxwell's equations under quasistatic conditions. For this, we utilize the versatile MNPBEM toolbox [34]. The torus is placed with its axis along the z direction. The particle is illuminated by a plane wave polarized in the z direction. We plot the scattering and extinction cross sections in Fig. 11 for a torus of aspect ratio

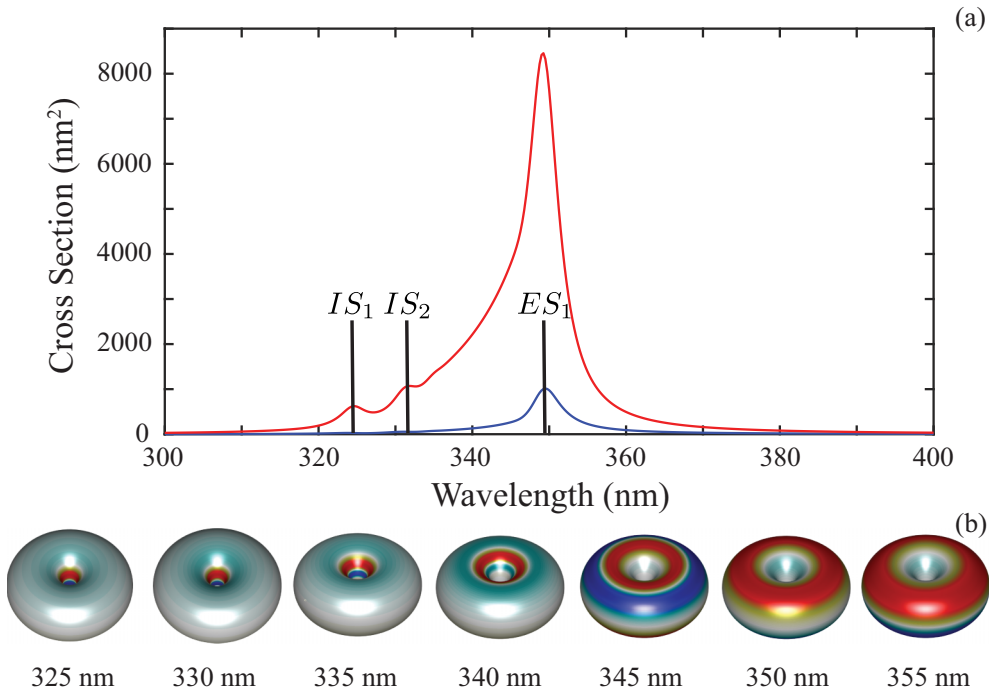

FIG. 11. (a) The scattering (blue) and extinction (red) cross sections for a torus with aspect ratio $\xi = 0.8$. The locations of some of the lowest order dipole active E and I modes are indicated by vertical bars. (b) The actual charge distributions as derived from solving Maxwell's equations under quasistatic conditions at various wavelengths.

0.8. To model particle properties we use the experimental permittivity values for silver as obtained from [35]. We fit that data into a Drude model and use the parameters uncovered to model the silver material. The ω_C for silver in this model lies near 343 nm. The frequencies predicted for the lowest order I and E modes by the numerical solution of the adjoint-NP equations are also indicated in the figure. The extinction peaks correspond exactly to the dipole-active lowest order modes. As expected due to the higher dipole moment, the ES_1 mode dominates the spectrum. The IS_1 and IS_2 modes are also sufficiently detuned to be visibly separate. The rest of the E and I modes are overshadowed by the ES_1 mode response. For higher aspect ratios, more I modes emerge from the shadow of the ES_1 mode. However, the dipole moments of the I modes decrease rapidly at higher aspect ratios causing the overall response to diminish. Simultaneously, the height of the ES_1 peak decreases with aspect ratio, allowing I modes to stand out. Hence, as far as the utility of the dipole-active I modes go, a balance needs to be stricken between obtaining a higher dipole moment and ensuring that the mode is sufficiently detuned to be visible individually. This balance occurs around $\xi = 0.4$ to $\xi = 0.8$ for the IS_1 mode.

We also study the actual induced charge distributions at each of the extinction frequency levels. As can be seen, at 325 nm, near the IS_1 resonance, the charge distribution looks exactly like the IS_1 distribution before moving into looking like the IS_2 distribution at 335 nm. We see a dramatic change with the change distribution moving from the inside to the outside near $\omega_C = 10$ nm. Near the ES_1 resonance at 350 nm, due to the interference of multiple higher order E modes, the charge distribution actually looks similar to that of a transverse cylinder mode. Near 355 nm, we recover the expected charge distribution for the ES_1 mode. We note that while the ES_1 mode lies in the middle of multiple other dark and bright modes (as shown in Fig. 10), due to its extremely high dipole moment, the E mode dominates the interaction pattern of the torus with light polarized in the z direction.

V. CONCLUSION

In this paper, we have completely deconstructed the structure of poloidal modes on a torus and subsequently completed our understanding of plasmonic modes on a torus. To this end, we have analytically derived an equation describing the negative eigenvalue surface charge poloidal modes on a torus and numerically shown the existence of an additional positive eigenvalue mode set. We show that these modes converge to the transverse cylindrical modes in the small aspect ratio limit. Hence, we have demonstrated that the two sets of modes may be considered as arising from the splitting of the transverse cylindrical modes due to the symmetry breaking that occurs when a cylinder is folded to form a torus. We conclude with a discussion of the actual modes that arise at specific frequencies by solving Maxwell's equations under planar wave illumination. We show that the modal analysis is actually useful in describing the extinction cross sections despite the nonorthogonality of the poloidal modes.

A key feature of the modes we derive is the spatial localization of the charge oscillations. The I modes and their electric fields are more intense on the inner portions of the torus while the E modes are more effective on the outer surface. The fact

that these modes are also separated in frequency space allows for frequency tuning of the spatial electric field profile. This is a feature not present in simple nanostructures such as spheres and rods. The actual frequency separation between the E and I modes is also tunable through modifications of the aspect ratio of the torus. We hope to investigate possible applications of these frequency-tunable, spatially separated modes in the future.

Another intriguing area for future investigation is the structure of plasmon modes on objects made by revolving a 2-dimensional shape around a fixed center. These objects can be thought of as being created by folding an infinite cylinder with a certain cross section. For example, consider an elliptic cylinder (a cylinder with an elliptical cross section). Folding the cylinder, we can create a shape similar to a torus but with an elliptical cross section. However, the regular cylinder has a continuous rotation symmetry around its axis. This means that the cylinder may be rotated by any angle around the axis and the resulting shape looks identical to the cylinder. However, for the elliptic cylinder, the cylinder may only be rotated by multiples of π radians to arrive at the same shape. The elliptic cylinder thus possesses a discrete symmetry around its axis. Thus, when the elliptic cylinder is folded to create a torus-like shape, it results in the breaking of a discrete symmetry instead of a continuous symmetry. We suggest that studying the effects of the breaking of such discrete symmetries would prove most interesting. Such investigations would lead to a much better understanding of plasmon modes on surfaces of revolution.

We finally note here that the analyses presented in this paper have been made in the electrostatic limit and will not be valid when the size of torus particles are comparable to the wavelength of light. However, in recent years, the synthesis of nanotori of extremely small dimensions has been successfully performed using novel techniques [36,37] for various applications.

ACKNOWLEDGMENTS

T.W.'s work was generously supported by the Monash University Postgraduate Publication Award.

APPENDIX: THE TOROIDAL COORDINATE SYSTEM

1. Transformation equations for toroidal coordinates

The toroidal coordinates can be depicted as shown in Fig. 2. The transformation equations from toroidal coordinates (ξ, η, ϕ) to the rectangular coordinates (x, y, z) can be given as

$$x = \frac{r_0\sqrt{1-\xi^2}\cos(\phi)}{1-\xi\cos(\eta)}, \tag{A1a}$$

$$y = \frac{r_0\sqrt{1-\xi^2}\cos(\phi)}{1-\xi\sin(\eta)}, \tag{A1b}$$

$$z = \frac{-r_0\xi\sin(\eta)}{1-\xi\cos(\eta)}. \tag{A1c}$$

The inverse transformation can be given as

$$\phi = \arctan\left(\frac{y}{x}\right), \tag{A2a}$$

$$\xi = \frac{2d_1d_2}{d_1^2+d_2^2}, \tag{A2b}$$

$$\eta = \arccos\left(\frac{d_1^2+d_2^2-4r^2}{2d_1d_2}\right), \tag{A2c}$$

where $d_1^2 = (\rho+r)^2+z^2$, $d_2^2 = (\rho-r)^2+z^2$, and $\rho^2 = x^2+y^2$.

2. The scale factors

The scale factors for the orthogonal toroidal coordinates can be given as

$$h_\xi = \frac{r_0}{\sqrt{1-\xi^2}[1-\xi\cos(\eta)]}, \tag{A3a}$$

$$h_\eta = \frac{r_0\xi}{1-\xi\cos(\eta)}, \tag{A3b}$$

$$h_\phi = \frac{r_0\sqrt{1-\xi^2}}{[1-\xi\cos(\eta)]}. \tag{A3c}$$

3. The normal vector

The normal vectors to the surfaces of constant ξ (surface of a torus) can be given by

$$\mathbf{n} = \left\{\frac{(\cos(\eta)-\xi)\cos(\phi)}{1-\xi\cos(\eta)}, \frac{[\cos(\eta)-\xi]\sin(\phi)}{1-\xi\cos(\eta)}, -\frac{\sqrt{1-\xi^2}\sin(\eta)}{1-\xi\cos(\eta)}\right\}. \tag{A4}$$

4. The inverse distance

The inverse distance between two points on a surface of constant ξ is

$$\frac{1}{|\mathbf{x_1}-\mathbf{x_2}|} = \frac{1}{\sqrt{2}r_0}\sqrt{\frac{[1-\xi\cos(\eta_1)][1-\xi\cos(\eta_2)]}{1-\xi^2\cos(\eta_1-\eta_2)-(1-\xi^2)\cos(\phi_1-\phi_2)}}. \tag{A5}$$

[1] M. I. Stockman, Nanoplasmonics: Past, present, and glimpse into future, Opt. Express **19**, 22029 (2011).

[2] S. Nie and S. R. Emory, Probing single molecules and single nanoparticles by surface-enhanced Raman scattering, Science **275**, 1102 (1997).

[3] H. A. Atwater and A. Polman, Plasmonics for improved photovoltaic devices, in *Materials for Sustainable Energy: A Collection of Peer-Reviewed Research and Review Articles from Nature Publishing Group* (World Scientific, London, 2011), pp. 1–11.

[4] E. I. Galanzha, R. Weingold, D. A. Nedosekin, M. Sarimollaoglu, J. Nolan, W. Harrington, A. S. Kuchyanov, R. G. Parkhomenko, F. Watanabe, Z. Nima *et al.*, Spaser as a biological probe, Nat. Commun. **8**, 15528 (2017).

[5] V. Senevirathne, H. Hapuarachchi, S. Mallawaarachchi, S. D. Gunapala, M. I. Stockman, and M. Premaratne, Scattering characteristics of an exciton-plasmon nanohybrid made by coupling a monolayer graphene nanoflake to a carbon nanotube, J. Phys.: Condens. Matter **31**, 085302 (2019).

[6] H. Hapuarachchi and M. Premaratne, Thermoresponsive nanohybrids for tumor imaging, in *2018 IEEE 12th International Conference on Nano/Molecular Medicine and Engineering (NANOMED)* (IEEE, Waikiki Beach, HI, 2018), pp. 20–24.

[7] K.-Y. Jung, F. L. Teixeira, and R. M. Reano, Au/SiO_2 nanoring plasmon waveguides at optical communication band, J. Lightwave Technol. **25**, 2757 (2007).

[8] D. Weeraddana, M. Premaratne, S. D. Gunapala, and D. L. Andrews, Controlling resonance energy transfer in nanostructure emitters by positioning near a mirror, J. Chem. Phys. **147**, 074117 (2017).

[9] M. Premaratne and M. I. Stockman, Theory and technology of spasers, Adv. Opt. Photonics **9**, 79 (2017).

[10] B. Liu, W. Zhu, S. D. Gunapala, M. I. Stockman, and M. Premaratne, Open resonator electric spaser, ACS Nano **11**, 12573 (2017).

[11] T. Warnakula, M. I. Stockman, and M. Premaratne, Improved scheme for modeling a spaser made of identical gain elements, J. Opt. Soc. Am. B **35**, 1397 (2018).

[12] D. Lelwala Gamacharige, S. D. Gunapala, M. I. Stockman, and M. Premaratne, Significance of the nonlocal optical response of metal nanoparticles in describing the operation of plasmonic lasers, Phys. Rev. B **99**, 115405 (2019).

[13] T. Warnakula, S. D. Gunapala, M. I. Stockman, and M. Premaratne, Cavity quantum electrodynamic analysis of spasing in nanospherical dimers, Phys. Rev. B **100**, 085439 (2019).

[14] G. Mie, Beiträge zur optik trüber medien, speziell kolloidaler metallösungen, Ann. Phys. **330**, 377 (1908).

[15] I. D. Mayergoyz, D. R. Fredkin, and Z. Zhang, Electrostatic (plasmon) resonances in nanoparticles, Phys. Rev. B **72**, 155412 (2005).

[16] J. Aizpurua, P. Hanarp, D. S. Sutherland, M. Käll, G. W. Bryant, and F. J. Garcia de Abajo, Optical Properties of Gold Nanorings, Phys. Rev. Lett. **90**, 057401 (2003).

[17] A. Mary, A. Dereux, and T. L. Ferrell, Localized surface plasmons on a torus in the nonretarded approximation, Phys. Rev. B **72**, 155426 (2005).

[18] F. Safford, Solution of Laplace's equation in toroidal coördinates deduced by a method of imaginary inversion, Ann. Math. **12**, 27 (1898).

[19] J. D. Love, Quasi-static modes of oscillation of a cold toroidal plasma, J. Plasma Phys. **14**, 25 (1975).

[20] K. Avramov, T. Ivanov, and I. Zhelyazkov, High-frequency surface waves on a toroidal isotropic plasma, Plasma Phys. Controlled Fusion **35**, 1787 (1993).

[21] M. Salhi, Surface plasmon modes in toroidal nanostructures and applications, Ph.D. thesis, University of Tennessee, Knoxville, 2016.

[22] K. V. Garapati, M. Salhi, S. Kouchekian, G. Siopsis, and A. Passian, Poloidal and toroidal plasmons and fields of multilayer nanorings, Phys. Rev. B **95**, 165422 (2017).

[23] C. M. Dutta, T. A. Ali, D. W. Brandl, T.-H. Park, and P. Nordlander, Plasmonic properties of a metallic torus, J. Chem. Phys. **129**, 084706 (2008).

[24] K. Ando, Y.-G. Ji, H. Kang, D. Kawagoe, and Y. Miyanishi, Spectral structure of the Neumann-Poincaré operator on tori, *Annales de l'Institut Henri Poincaré C, Analyse non linéaire* (Elsevier, 2019).

[25] R. A. Johnson, *Advanced Euclidean Geometry* (Courier Corporation, New York, 2013).

[26] J. W. Bates, On toroidal Green's functions, J. Math. Phys. **38**, 3679 (1997).

[27] C. Neumann, *Über die Methode des Arithmetischen Mittels* (S. Hirzel, Leipzig, 1887).

[28] H. Poincaré *et al.*, La méthode de neumann et le probleme de dirichlet, Acta Math. **20**, 59 (1897).

[29] F. Ouyang and M. Isaacson, Surface plasmon excitation of objects with arbitrary shape and dielectric constant, Philos. Mag. B **60**, 481 (1989).

[30] D. R. Fredkin and I. D. Mayergoyz, Resonant Behavior of Dielectric Objects (Electrostatic Resonances), Phys. Rev. Lett. **91**, 253902 (2003).

[31] O. D. Kellogg, *Foundations of Potential Theory* (Courier Corporation, New York, 1953).

[32] A. C. Pipkin, *A Course on Integral Equations* (Springer Science & Business Media, New York, 1991).

[33] Y.-G. Ji and H. Kang, A concavity condition for existence of a negative value in Neumann-Poincaré spectrum in three dimensions, Proc. Am. Math. Soc. **147**, 3431 (2019).

[34] U. Hohenester and A. Trügler, MNPBEM: A Matlab toolbox for the simulation of plasmonic nanoparticles, Comput. Phys. Commun. **183**, 370 (2012).

[35] Y. Jiang, S. Pillai, and M. A. Green, Realistic silver optical constants for plasmonics, Sci. Rep. **6**, 30605 (2016).

[36] Y. Yan, P. Padmanabha Pillai, J. V. Timonen, F. S. Emami, A. Vahid, and B. A. Grzybowski, Synthesis of toroidal gold nanoparticles assisted by soft templates, Langmuir **30**, 9886 (2014).

[37] A. Steinhaus, R. Chakroun, M. Müllner, T.-L. Nghiem, M. Hildebrandt, and A. H. Gröschel, Confinement assembly of ABC triblock terpolymers for the high-yield synthesis of Janus nanorings, ACS Nano **13**, 6269 (2019).